Implications of Arctic sea ice changes for North Atlantic deep convection and the meridional overturning circulation in CCSM4-CMIP5 simulations

Alexandra Jahn[1] and Marika M. Holland[1]

Received 27 November 2012; revised 9 January 2013; accepted 21 January 2013; published 26 March 2013.

[1] Using CCSM4 climate simulations for 1850–2300 with four different future forcing scenarios, we show that the maximum strength of the Atlantic meridional overturning circulation (MOC) decreases proportionally to the applied CO_2 forcing. This weakening of the overturning is caused by a reduction or shut down of North Atlantic (NA) deep convection due to a surface freshening. In the Labrador Sea, the surface freshening is caused by strongly increased liquid freshwater exports from the Arctic, which are largely due to the decrease in the Arctic sea ice cover. In the strongest forcing scenario (RCP8.5), the Arctic becomes summer ice-free by the end of the 21st century and year-round ice-free by the end of the 23rd century. As a result of the associated freshening, all NA deep convection ceases by 2145, which leads to a 72% (18 Sv) decrease of the MOC strength by the end of the simulation in 2300. **Citation:** Jahn, A., and M. M. Holland (2013), Implications of Arctic sea ice changes for North Atlantic deep convection and the meridional overturning circulation in CCSM4-CMIP5 simulations, *Geophys. Res. Lett.*, *40*, 1206–1211, doi:10.1002/grl.50183.

1. Motivation

[2] To explore the long-term climate impacts of the different emission scenarios (called representative concentration pathways or RCPs) used in the Coupled Model Intercomparison Project Phase 5 (CMIP5), some modeling centers extended the CMIP5 simulations to the year 2300. The CO_2 forcing used in these simulations is shown in Figure 1a (see *Meinshausen et al*. [2011], for details on the forcing of these RCP extension simulations). In several of the CMIP5 models, the strength of the MOC in these RCP simulations shows a reduction in response to the increasing CO_2 forcing, but no abrupt shut down [*Weaver et al*., 2012] Similar results are found in the Community Climate System model version 4 (CCSM4), which shows a reduction of the MOC in all RCPs, with a reduction of up to 72% by 2300 in the strongest emission scenario, the RCP8.5 [*Meehl et al*., 2012]. This reduction occurs at atmospheric CO_2 levels of 1962 ppm, with globally averaged surface temperatures 8°C above 1986–2000 levels and a year-round ice-free Arctic Ocean [see Figures 9, 15, and 19 in *Meehl et al*., 2012]. Here we investigate the reasons for the simulated MOC reductions and link it to the simulated changes in the Arctic sea ice cover in the CCSM4 RCP simulations and their extensions to 2300, demonstrating the important potential downstream impacts of changes in the Arctic Ocean under the CMIP5 forcing scenarios.

2. Methods

[3] We use CMIP5 ensemble simulations with the CCSM4 model, which is a configuration of the Community Earth System Model (CESM) family of models [*Gent et al*., 2011]. CCSM4 is a fully coupled climate model with a nominal resolution of $0.9° \times 1.25°$ in the atmosphere and land models and 1° in the ocean and sea ice models. Its components and simulations have been described in a large collection of articles, many of them contained in a special collection in the *Journal of Climate* (http://journals.ametsoc.org/page/CCSM4/CESM1). In particular, it has been shown that the CCSM4's representation of late 20th century Arctic atmospheric [*de Boer et al*., 2012] and sea ice processes [*Jahn et al*., 2012; *Kay et al*., 2011] compares reasonably well with observations. Note that the CCSM4 simulations do not include an active ice sheet model, so impacts of ice-sheet melting in Greenland are not accounted for.

[4] The simulations used here consist of six ensemble members for the historical period (1850–2005), six ensemble members for 2005–2100 for each RCP (2.6, 4.5, 6.0, 8.5), and one ensemble member for each extended RCP scenario (for 2101–2300). The global climate in these CCSM4 simulations has been analyzed by *Meehl et al*. [2012]. Note that for RCP8.5, data are missing due to a damaged data storage tape between 2235 and 2241 (shown as gap in the graphs). Freshwater (FW) fluxes and storage are calculated relative to a mean salinity of 34.8 practical salinity unit (psu), and details on the FW calculations and the Arctic FW budget in the CCSM4 20th century simulations can be found in *Jahn et al*. [2012]. The Atlantic MOC index is calculated as the maximum of the annual-mean Atlantic stream function below 500 m in the northern Hemisphere, including both the Eulerian mean and the additional components. The sea-ice extent is calculated as the area covered by at least 15% ice concentration.

3. Arctic Changes

3.1. Arctic Sea Ice

[5] The Arctic sea ice extent decreases proportionally to the radiative forcing in all RCPs (once interannual variability is smoothed out through a 20 year running mean, see Figure 1d). September ice-free conditions of less than 1 million km^2 are simulated at the end of the 21st century in RCP8.5 and in the early 22nd century in RCP6.0 (see Figure 1b). At less than 1 million km^2 of sea ice extent, the Arctic Ocean is ice-free for

[1]National Center for Atmospheric Research, Boulder, Colorado, USA.

Corresponding author: A. Jahn, National Center for Atmospheric Research, 1850 Table Mesa Drive, Boulder, CO 80305, USA. (ajahn@ucar.edu)

0094-8276/13/10.1002/grl.50183

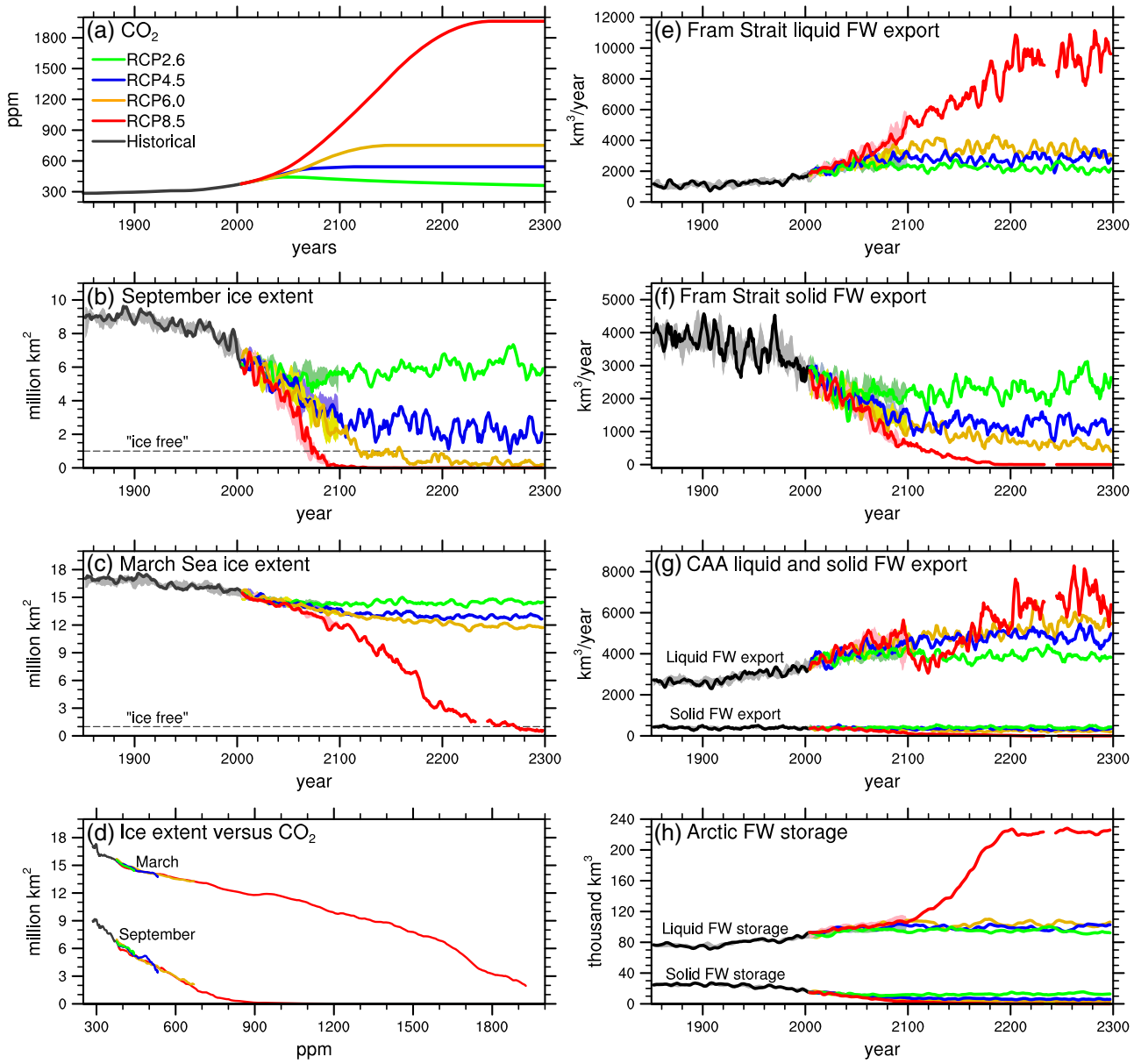

Figure 1. Time series of the (a) annual CO_2 forcing in the CMIP5 RCP simulations, the Arctic sea ice extent in (b) September and (c) March, the annual Fram Strait (e) liquid and (f) solid FW export, (g) the annual CAA liquid and solid FW export (as marked in the panel), and (h) the annual mean Arctic FW storage (liquid FW in the top 250 m and solid FW, as marked in the panel). Figure 1d shows the 20 year running mean of the sea ice extent from Figures 1b and 1c versus the increasing CO_2 forcing in one ensemble member of the RCP simulations. The 20 year running mean is used to smooth out the interannual variability, which we do not expect to be forced by CO_2. As we want to show the transient response of the sea ice extent to the CO_2 increase, Figure 1d shows the relationship until the CO_2 forcing stabilizes or reaches its maximum (see Figure 1a). All panels except Figures 1a and 1d show 5 year running means and show one ensemble member as thick line, with shading indicating the ensemble spread between 1850 and 2100, when multiple members are available.

all practical purposes, with the remaining sea ice located north of Greenland and in the narrow channels of the CAA. Wintertime sea ice extents also decline over the 21st century in all RCP scenarios, but only RCP8.5 with its increasing radiative forcing past 2150 shows a drastic decline in the winter sea ice extent, leading to year-round ice-free conditions by the end of the 23rd century (Figure 1c). We find that the climatic evolution of sea ice and many other properties are largely determined by the CO_2 level, not the trajectory by which that level was reached. As such, a similar transient climate response is seen for all RCPs when assessing changes as function of the increasing CO_2 level. Once the CO_2 levels stabilize or begin to decline, the climate begins to adjust to the new stable conditions and departs from the transient climate state proportional to the CO_2 level. As our focus is mainly on the transient response of the climate to the increasing CO_2 forcing in the CMIP5 scenarios, we focus on results from the RCP8.5 scenario runs in the following, as these simulations prescribe CO_2 levels that encompass and far exceed the CO_2 levels in the other scenarios.

3.2. Arctic Freshwater Export

[6] The large simulated changes in the Arctic sea ice extent and volume have a wide range of impacts, but here we concentrate on the resulting changes in the Arctic FW export and the downstream impacts on the deep water formation (section 4). As shown in Figures 1e–1g, the impact on the simulated FW export to the NA through the two main pathways (Fram Strait and CAA) is a shift toward more and more FW export in the liquid phase, as well as a general increase in the total FW export. The simulated phase change of the FW export is important for downstream effects, as the FW in liquid and solid form reaches different regions (see section 4).

[7] The large increase in the liquid FW export in RCP8.5 reflects a significant freshening of the outflow between the early 21st century and the early 23rd century (by 2.5 psu in Fram Strait and 4.5 psu in the CAA). Between 2005 and 2200, this freshening of the Arctic Ocean (Figure 1h) is caused by increased sea ice melt within the Arctic and reduced sea-ice formation and export (53%), as well as by increased FW input from rivers (28%), an increase in the FW import through Bering Strait (16%), and increased net precipitation (2%) due to a generally enhanced hydrological cycle in a warmer climate.

[8] While the salinity of the outflow decreases, the volume of the liquid FW export through the CAA and Fram Strait in RCP8.5 declines by up to 50% during the late 21st and the mid 22nd century, respectively. For the CAA, the impact of the decrease in the volume export can be seen around 2100 as an intermittent reduction in the RCP8.5 liquid FW export in Figure 1g. It is caused by the shutdown of the deep convection in the Labrador Sea at this time (see section 4) and the associated rise in sea surface height in the Labrador Sea, which reduces the sea surface height gradient to the Arctic that drives this export (see *Jahn et al.* [2010] and *Houssais and Herbaut* [2011] for details of this mechanism). This decrease in the CAA liquid FW export leads to a sharp increase in the Arctic liquid FW storage after 2100 (Figure 1h). For Fram Strait, the volume flux decrease is fully compensated by the freshening of the outflow, so it cannot be seen in Figure 1e. It occurs around 2145, after the shutdown of the deep convection in the Nordic Seas, and is caused by the associated sea surface height gradient change across the East Greenland current after deep convection ceases (see *Jahn et al.* [2010], for details of this mechanism).

4. Impacts on Deep Convection and MOC

4.1. Deep Convection Impacts

[9] The large increase in the liquid FW export from the Arctic at the end of the 21st century in RCP8.5 leads to a shutdown of February–April (FMA) deep convection in the Labrador Sea deep convection region at the start of the 22nd century (shown as white box in Figure 2a, maximum depth of deep convection is shown in Figure 2b). Before a complete shutdown of Labrador Sea deep convection occurs in RCP8.5, several abrupt reductions of deep convection occur in all six ensemble members of RCP8.5 at the end of the 21st century. They occur in response to decreased sea surface salinity (SSS) in the same region (see Figures 3b and 3c), with a correlation between the maximum depth of deep convection and the SSS in the same region of between 0.90 and 0.95 in the different ensemble members ($p > 0.95$,

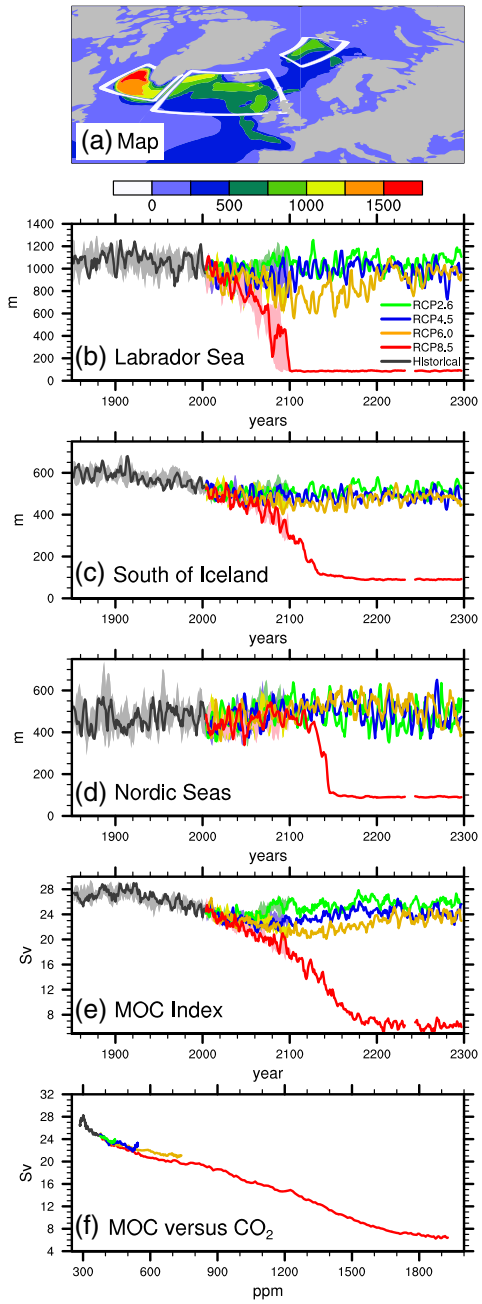

Figure 2. Wintertime (February–April) depth of (a–d) maximum deep convection and (e–f) Atlantic MOC index. The spatial distribution of maximum deep convection is shown in Figure 2a, averaged over 1981–2005 in one ensemble member. The evolution over time (smoothed by a 5 year running mean) averaged over each of the three main deep convection regions in the model (shown as white boxes in Figure 2a) is shown in Figures 2b–2d. The continuous ensemble member for 1850–2300 is shown as thick line. Shading for years 1850–2100 shows the range of the other five ensemble members. The 5 year running mean of the Atlantic MOC index [SV] is shown in Figure 2e. In Figure 2f, the 20 year running mean of the Atlantic MOC index is shown as function of the CO_2 forcing used in the different RCPs (see Figure 1a), for one ensemble member for each of the four extended RCPs. As in Figure 1d, we only show the relationship until the CO_2 forcing stabilizes or reaches its maximum.

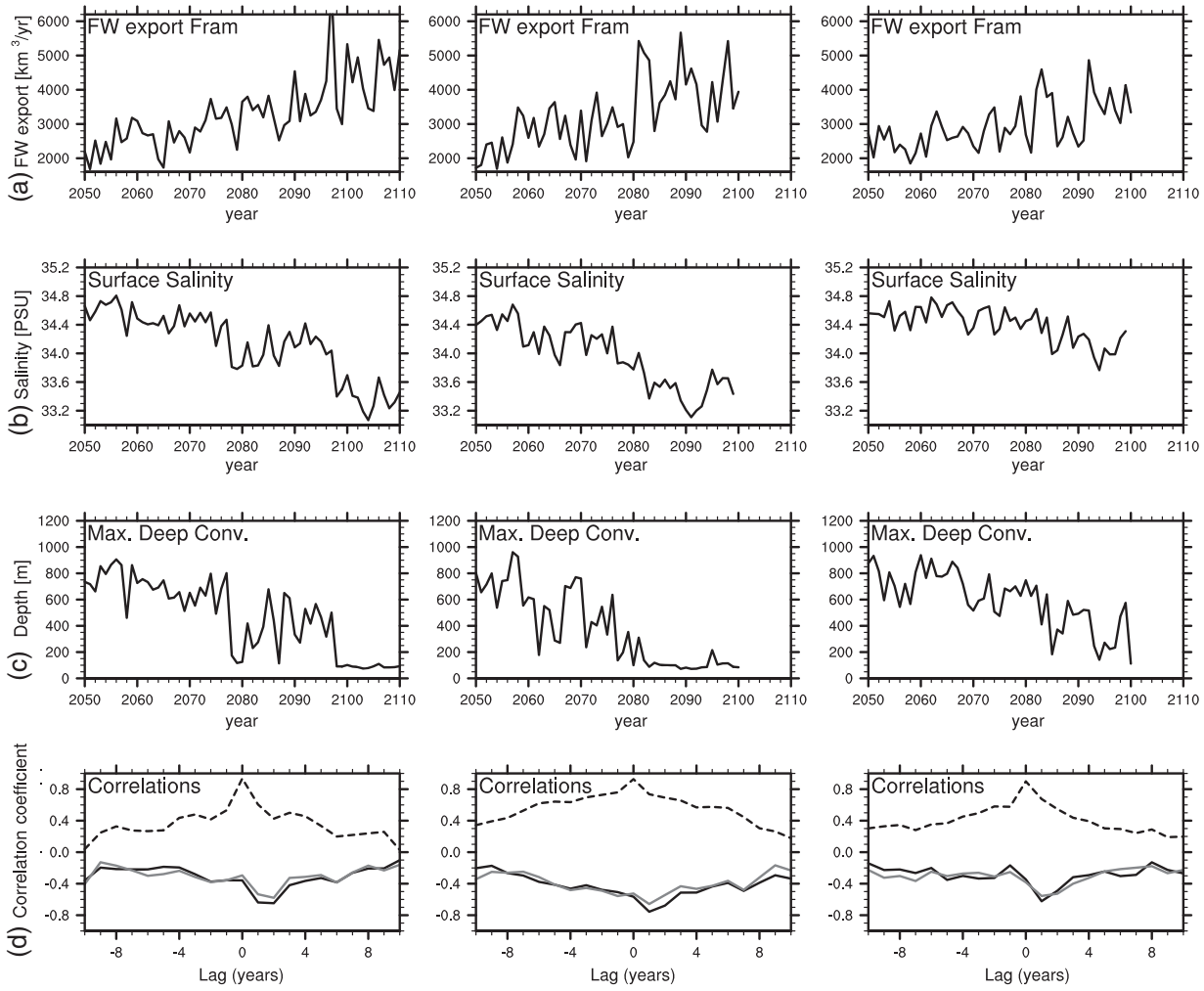

Figure 3. Wintertime (February–April) (a) Fram Strait liquid FW export, (b) Labrador Sea Surface Salinity (SSS), (c) Labrador Sea maximum depth of deep convection, and (d) lagged correlations between these three time series for 2050–2100 for three ensemble members of the RCP8.5 simulations with the CCSM4. The first ensemble member on the left is the one that was extended to 2300. The other two ensemble members are examples of the range of the evolution in the different ensemble members. In Figure 3d, the black dashed line shows the correlation between the FMA Labrador SSS and the maximum level of deep convection, the solid black line shows the correlation between the Fram Strait FW export and the Labrador Sea SSS, and the grey line shows the correlation between the Fram Strait liquid FW export and the maximum level of deep convection.

see Figure 3d). We find that deep convection always ceases when the FMA SSS drops below 33.8–34 psu (see Figures 3b, 3c, and 4e), while the FMA sea surface temperatures during these abrupt reductions of deep convection vary between 1°C and 5°C. We find that the Labrador Sea SSS changes are controlled to a large extent by the liquid FW export through Fram Strait, which affects the Labrador Sea SSS with a lag of 1 year. This is shown by a lagged-correlation analysis with correlations at 1 year lag between −0.59 and −0.87 for the different ensemble members ($p > 0.95$; see Figure 3d). The solid Fram Strait FW export does not have a strong impact on Labrador Sea SSS, as most of it does not reach the interior of the Labrador Sea.

[10] The FW export through the channels of the CAA does not show an impact on the SSS or deep convection in the Labrador Sea (not shown). This is in line with results from other model studies that showed that the FW export from the CAA does not reach the interior of the Labrador Sea [e.g., *Myers*, 2005; *Houssais and Herbaut*, 2011]. We do, however, find a positive correlation of up to 0.77 ($p > 0.95$) between the CAA FW export and the Labrador Sea deep convection at zero-year lag. This correlation is caused by the impact of sea surface height variations in the Labrador Sea on the volume flux through the CAA, as described in section 3.

[11] Deep convection south of Iceland and in the Nordic Seas shuts down during the first part of the 22nd century in RCP8.5, but shows no large changes in the other RCPs (Figures 2c and 2d). In RCP8.5, the reduction of deep convection to below 200 m again occurs when the local SSS drops below 33.8–34 psu (see Figure 4), as already seen in the Labrador Sea. The deep convection south of Iceland stops first (around 2120), followed by the deep convection in the Nordic Seas about 25 years later (around 2145, see Figures 2c, 2d, and 4).

[12] In contrast to the Labrador Sea, there is no significant correlation between the SSS and the FW export from the Arctic. Instead, the surface freshening occurs as a result of a decreased northward flux of salty Atlantic water. This is due to the changes in the NA ocean circulation after the Labrador Sea deep water formation (and later the deep water

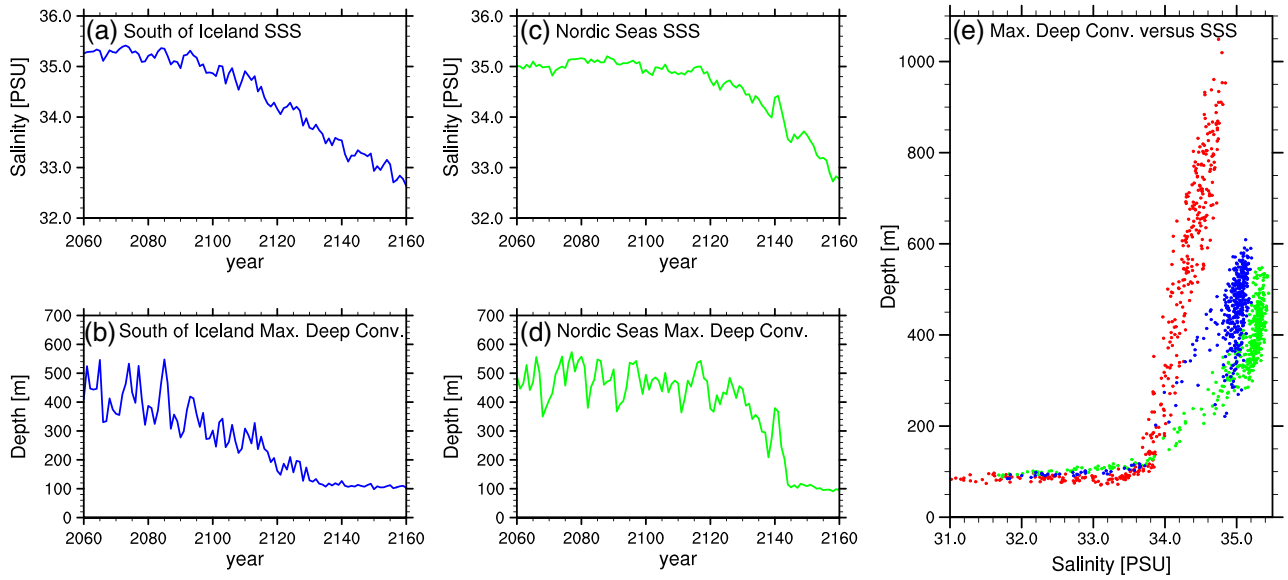

Figure 4. Wintertime (February–April) (a and c) sea surface salinity and (b and d) maximum level of deep convection averaged over the deep convection regions south of Iceland (Figures 4a and 4b) and in the Nordic Seas (Figures 4c and 4d) for 2060–2160 in one ensemble member of the RCP8.5 simulation. Figure 1e shows the maximum depth of deep convection in the Labrador Sea (red), south of Iceland (blue), and in the Nordic Seas (green) as a function of surface salinity for 2050–2179 in all available ensemble members of RCP8.5.

formation south of Iceland) stops and the MOC index weakens (Figure 2e). This reduced northward flux of salty water is consistent with previous work that describes the impact of changes in the subpolar gyre circulation on the inflow into the Nordic Seas [*Hátún et al*., 2005]. It is also consistent with the general shift toward a more positive Northern Annular Mode during the course of the RCP8.5 simulation [*Meehl et al*., 2012], which has been linked to a freshening in the Nordic Seas due to an intensification of the subpolar gyre [*Richter and Maus*, 2011].

4.2. MOC Impacts

[13] As the MOC represents the integrated effects of deep convection from different sites and of the large-scale ocean circulation in general, the Atlantic MOC index shows no abrupt changes, despite the abrupt shutdown of deep convection in some of the NA deep convection sites (Figure 2e). Instead it gradually weakens to 7 Sv (28% of its 20th century value of 25 Sv) by 2200, as deep convection in all three NA convection sites ceases and the MOC spins down. This decrease of the MOC strength is again proportional to the transient CO_2 forcing once interannual variability is smoothed out (Figure 2f). A reduction in MOC strength is therefore observed for all RCPs while the CO_2 increases. In RCP2.6, RCP4.5, and RCP6.0, the MOC index recovers within one to three decades after the CO_2 forcing decreases or stabilizes and the salinity anomalies are flushed out of the deep convection regions. In RCP8.5, however, the stabilization in 2250 does not lead to a similarly fast recovery, as the water column in the deep convection regions is too stable to erode quickly.

5. Conclusions

[14] The results from the RCP ensemble simulations with the CCSM4 and their single-ensemble member extensions to 2300 show that the large simulated changes in the Arctic sea ice have impacts on the NA deep convection and the strength of the MOC, through changes in the Arctic FW export. We find that the response of the simulated sea ice cover, FW export, Labrador Sea deep convection, and Atlantic MOC index is proportional to the CO_2 forcing in the RCP simulations (until stabilization of the CO_2 forcing), with similar values obtained across the different scenarios when they reach the same CO_2 level. This indicates that the rate of CO_2 changes does not strongly influence the transient climate response. We therefore focused our analysis on the strongest forcing scenario, the RCP8.5 simulation. It shows a summer ice-free Arctic by the end of the 21st century and a year-round ice-free Arctic by the end of the 23rd century. The associated freshening of the Arctic Ocean and the loss of the Arctic sea ice cover lead to an increased liquid FW export, while the solid FW export decreases strongly. The associated freshening of the Labrador Sea causes a shutdown of Labrador Sea deep convection by the end of the 21st century. The deep convection in the other NA deep convection sites ceases by 2145, leading to a slow reduction of the Atlantic MOC to 7 Sv (28% of its 20th century value). The resulting decrease of the northward oceanic heat transport causes a 2°C cooling over the NA between the end of the 21st and the end of the 22nd century [Figure 11 in *Meehl et al*., 2012]. A net cooling over land in northern Europe is not simulated in RCP8.5, due to the very strong global warming simulated in the extended RCP8.5 simulation, which offsets most of the cooling associated with the reduced ocean heat transport to high latitudes. While these results are from only one model, a large reduction of the MOC index and the absence of abrupt changes in the MOC are seen in RCP8.5 extension simulations with at least two other CMIP5 models [*Weaver et al*., 2012].

[15] **Acknowledgments.** We thank G. Strand for making the RCP extension output available. Helpful comments from P. Gent (NCAR) and two anonymous reviewers are appreciated. A. Jahn was supported by a

postdoctoral fellowship from ASP at NCAR. NCAR is sponsored by NSF. The CESM project is supported by NSF and BER at DOE. Computing resources were provided by CSL at NCAR's CISL, sponsored by NSF and other agencies. The extended RCP simulations were run at NCCS at ORNL and at NERSC, which are supported by BER at DOE under contracts DE-AC05-00OR22725 and DE-AC02-05CH11231, respectively. Figures were plotted using NCL (http://dx.doi.org/10.5065/D6WD3XH5).

References

de Boer, G., W. Chapman, J. Kay, B. Medeiros, M. D. Shupe, S. Vavrus, and J. Walsh (2012), A characterization of the Arctic atmosphere in CCSM4, *J. Climate*, *25*(8), 2676–2695, doi:10.1175/JCLI-D-11-00228.1.

Gent, P. R., et al. (2011), The Community Climate System Model version 4, *J. Climate*, *24*(19), 4973–4991, doi:10.1175/2011JCLI4083.1.

Hátún, A., A. B. Sandrø, H. Drange, B. Hansen, and H. Valdimarsson (2005), Influence of the Atlantic Subpolar Gyre on the thermohaline circulation, *Science*, *309*, 1841–1844, doi:10.1126/science.1114777.

Houssais, M.-N., and C. Herbaut (2011), Atmospheric forcing on the Canadian Arctic Archipelago freshwater outflow and implications for the Labrador Sea variability, *J. Geophys. Res.*, *116*, doi:10.1029/2010JC006323.

Jahn, A., L. B. Tremblay, R. Newton, M. M. Holland, L. A. Mysak, and I. A. Dmitrenko (2010), A tracer study of the Arctic Ocean's liquid freshwater export variability, *J. Geophys. Res.*, *115*, doi:10.1029/2009JC005873.

Jahn, A., et al. (2012), Late 20th century simulation of Arctic sea ice and ocean properties in the CCSM4, *J. Clim.*, *25*(5), 1431–1452, doi:10.1175/JCLI-D-11-00201.1.

Kay, J. E., M. M. Holland, and A. Jahn (2011), Inter-annual to multi-decadal Arctic sea ice extent trends in a warming world, *Geophys. Res. Let.*, *38*, doi:10.1029/2011GL048008.

Meehl, G. A., et al. (2012), Climate system response to external forcings and climate change projections in CCSM4, *J. Climate*, *25*(11), 3661–3683, doi:10.1175/JCLI-D-11-00240.1.

Meinshausen, M., et al. (2011), The RCP greenhouse gas concentrations and their extension from 1765 to 2300, *Clim. Chang.*, *109*(1–2), 213–241, doi:10.1007/s10584-011-0156-z.

Myers, P. G. (2005), Impact of freshwater from the Canadian Arctic Archipelago on Labrador Sea water formation, *Geophys. Res. Lett.*, *32*, doi:10.1029/2004GL022082.

Richter, K., and S. Maus (2011), Interannual variability in the hydrography of the Norwegian Atlantic Current: Frontal versus advective response to atmospheric forcing, *J. Geophys. Res.*, *116*, doi:10.1029/2011JC007311.

Weaver, A. J., et al. (2012), Stability of the Atlantic meridional overturning circulation: A model intercomparison, *Geophys. Res. Lett.*, *39*, doi:10.1029/2012GL053763.